Chaperone-mediated autophagy substrates bind to lid domain of Hsc70: Exploration using integrated approach

Devid Sahu[1], Nidhi Malhotra[1]*

[1] Department of Chemistry, School of Natural Sciences, Shiv Nadar Institution of Eminence, Gautam Buddha Nagar, Uttar Pradesh 201314, India

*Correspondence: nidhi.malhotra@snu.edu.in; ORCID: 0000-0002-0218-3440

Abstract

Chaperone-mediated autophagy (CMA) is a selective lysosomal degradation pathway crucial for cellular homeostasis. Its dysfunction is linked to cancer and neurodegenerative disorders. Hsc70 mediates CMA selectivity by recognizing proteins with 'KFERQ-type' sequences, but the structural basis for substrate recognition and the substrate-binding mechanism of Hsc70 remain unclear. This study integrates literature, bioinformatics, AlphaFold 3 predictions, and 29 μs of molecular dynamics (MD) simulations to elucidate the lid domain interactions of Hsc70 with fifteen verified CMA substrate segments. Structural and thermodynamic residue-level analyses suggest binding occur in a hydrophobic cavity formed by alpha helix α1 and α3 in the lid domain of hsc70, with complex stabilization primarily driven by hydrophobic residues within 'KFERQ-type' motif and its flanking regions. The robustness of our findings is confirmed by consistent convergence across force fields, substrates, and supporting literature, all identifying the same site. This study offers insights into therapeutic modulation of the CMA pathway.

Keywords: AlphaFold 3; Autophagy; HSC70; KFERQ-type motif; Lid domain; Molecular dynamic simulations; Substrate

Abbreviations: CMA: Chaperone-Mediated Autophagy; AF3: AlphaFold 3; MD: Molecular Dynamics; Hsc: Heat Shock Cognate; SBD: Substrate Binding Domain

Introduction

Chaperone-Mediated Autophagy (CMA) is a selective degradation process with diverse roles in maintaining cellular homeostasis, regulating immune response, influencing aging, and contributing to the pathogenesis of various diseases, including cancer[1–5]. The unique feature of selectivity distinguishes it from other types of autophagy. The selectivity is rendered by a heat shock cognate protein, Hsc70, that recognizes only a cohort of selective proteins called substrates and only such proteins are amenable to degradation by CMA. Despite its well-established function in recognizing and binding substrate proteins, the precise molecular details governing the interaction between Hsc70 and its substrate proteins remain largely unknown. Sequence-based designation of the substrate requires presence of 'KFERQ-type' motifs in them[6–9]. This motif typically includes one negatively charged residue (D or E), one or two positively charged residues (K or R) and one or two hydrophobic residues (I, L, V, or F) in any order along with a glutamine (Q) at either end of the motif. The "KFERQ-type" motif can be turned on or off by chemical changes to proteins i.e post-translational modifications (ubiquitination, phosphorylation or acetylation). KFERQ type motifs without any modifications are called canonical motifs[10–14]. Currently, ~80 protein substrates are known for CMA, of which 61 substrates have been identified in humans[14–21]. The challenge lies in deciphering how Hsc70 achieves specificity for substrate proteins in a cellular environment where multiple proteins bear similar recognition motifs. Particularly, what are the structural fingerprints that label a protein as a CMA substrate, how does hsc70 recognize those fingerprints, what is the substrate binding site in hsc70? This gap in understanding has significant implications, as substrate recognition is the cornerstone of CMA's selectivity, influencing various cellular processes and disease outcomes.

Hsc70 is a constitutive member of the Hsp70 family that shares a conserved structural architecture comprising of a nucleotide binding domain (NBD), and a substrate binding domain (SBD). The SBD is sub-divided into SBDβ, SBDα (lid) and a C-terminal extension[22,23]. Most of the existing literature exclusively utilized short peptides as model substrates to develop the current understanding of chaperone-substrate binding[24–27]. Crystal structure of a model peptide model NRLLLTG (NR) in complex with DnaK suggested that the peptide binds in an extended conformation in a canonical hydrophobic cleft within SBDβ[27]. Literature suggests that Hsc70 binds to the substrate protein containing KFERQ-type motifs at a site other than the canonical hydrophobic binding groove[28]. Non-canonical interaction is also expected owing to the polar nature of the motif. Peptides constituting CMA-targeting motifs of substrate protein 'Tau' were experimentally shown to bind independently and did not compete with model peptides for binding at SBD[29]. In the same study, NMR experiments have shown that these KFERQ-type peptide motifs were unable to bind Hsc70's SBD that contained only SBDβ. It raises the possibility of SBDα as a potential binding site. Moreover, SBDα is the sequentially divergent region amongst Hsp70 orthologs and binding at this site can account for the differential binding of tau with Hsc70 and Hsp72[30].

There are several bottlenecks towards gaining a comprehensive understanding of the interactions between Hsc70-substrate complex. Firstly, the atomistic structure of Hsc70 is unknown and the exact binding site is unidentified. Literature suggests binding at sites other than the canonical substrate binding cleft [28]. Additionally, consistent with the principle applicable to chaperones in general, its binding with the client protein must be strong enough to prevent the spontaneous detachment of the bound protein yet not so strong to enable its detachment for subsequent downstream events. Thus, these chaperone-client complexes are considered as "fuzzy" complexes.

The binding interfaces constitute formation of transient, dynamic, and nonspecific interactions, capable of modulating the conformational equilibrium, which are difficult to capture experimentally. The groundbreaking deep learning approach of AlphaFold 3 predicts structures of proteins and their complexes by leveraging evolutionary and structural data[31]. Combined with MD simulations, which model atomic interactions and dynamic motions, it provides a powerful framework to analyze these transient and dynamic interactions, overcoming experimental limitations. In the current study, we have utilized an integrated approach combining information from existing literature, bioinformatics, AlphaFold 3 and molecular dynamics simulations to predict hsc70-substrate binding interactions. Our findings suggest that the residues adjacent to the CMA-targeting motifs in the same secondary structure element stabilize the binding interactions between hsc70 and substrate. The analysis on these extended CMA-targeting motifs in fifteen human substrate proteins reveal common binding site on SBDα of Hsc70 encompassing residues Tyr545, Asn548, Thr552, Leu558, Lys561, Glu600, Ile607, Leu610, and Tyr611. The site consists of hydrophobic interior with hydrophilic residues flanking the central pocket. The use of various force fields, different substrates, and supporting evidence from existing literature—all converging on the same site—validates the robustness and success of our study.

Results and Discussion

Adjacent Residues contribute to the Stability of 'KFERQ-type' Motif Binding to Hsc70

The binding of Hsc70 to CMA substrates has primarily been studied at the sequence level to date, with the well-known recognition of 'KFERQ-type' motifs in substrates involved in binding. At the structural level, evidence from multiple sources in literature suggests binding at the lid domain/SBDα of hsc70 [28–30,32,33]. The site deviates from the canonical binding (SBDβ) paradigm that emerged from extensive analysis on substrate-binding mechanisms of Hsp70 family

members, including DnaK. This distinction might also reflect functional specialization, with Hsc70 accommodating CMA substrates that diverge from the canonical substrates recognized by DnaK. To understand the structural basis for substrate recognition and the substrate-binding mechanism to SBDα of Hsc70, we compiled a list of CMA substrates and analyzed their interaction with SBDα of Hsc70, focusing on the recognition of 'KFERQ-type' motif.

A comprehensive list of experimentally validated CMA substrates in humans was collated [SI Table 1]. Using the KFERQ Finder bioinformatics tool, both canonical KFERQ motifs and KFERQ-like motifs generated by post-translational modifications (PTMs) were identified[14]. Fifteen substrates containing a single canonical motif were selected for analyzing the recognition and binding site in hsc70 SBDα. The selected substrates are: RND3(Rho-related GTP-binding protein RhoE), Abeta(Amyloid-beta precursor protein), Annexin A1, Annexin A2, Annexin A6, GBA1(Lysosomal acid glucosylceramidase), Cyclin D1(G1/S-specific cyclin-D1), PEA15(Astrocytic phosphoprotein PEA-15), HBB(Hemoglobin subunit beta), CHK1(Serine/threonine-protein kinase Chk1), α-Synuclein, Annexin A4, Prion protein(Major prion protein), PKM(Pyruvate kinase PKM), and PARK7(Parkinson disease protein 7). AlphaFold 3 was utilized to predict the structure of the complex between the 'KFERQ-type' motif and SBDα of human hsc70. Figure 1A depicts the residues involved in the binding interface of hsc70. Majorly, three distinct sites were observed (site-1 is colored medium purple, site-2 as pink and site-3 as orange). Few representative protein complexes from each site (RND3, Abeta and Annexin A1 from site-1, CHK1, and PKM from site-2 and PARK7 from site-3) were subjected to all-atom MD simulations. The stability of the binding site was checked by plotting the minimum distance between the substrate and the receptor, Figure 1C and Fig. S1A. In all cases, the predicted binding site demonstrated structural instability during the simulations, failing to maintain its integrity

throughout the trajectory. Consequently, the substrate exhibited a loss of association with the putative binding pocket and migrated away from the predicted site. This dislocation suggests a potential need to refine the molecular environment to accurately replicate the native binding dynamics.

Since the 'KFERQ-type' motif alone does not maintain sufficient stability in complex with hsc70, we investigated the potential contribution of adjacent residues in stabilizing the motif's interaction with the chaperone, as their presence may be essential for effective binding. Extensive stabilization by additional residues outside the consensus sequence motifs have also been previously observed for LIR motifs [34,35]. This motif is flanked by C-helix residues that cause additional stabilization. To define 'adjacent' residues in our study, the subset of shortlisted substrate proteins is analyzed for the existence of secondary structural elements in 'KFERQ-type' sequence motifs (Figure 1D). It was observed that the motif forms a part of alpha-helical conformation in ten proteins. In only one and four proteins, on the other hand, the motif exists in beta-sheet and loop respectively. Those existing in the loop have flanking residues in alpha-helical conformation. Adjacent residues are defined as variable-length stretches of residues flanking the 'KFERQ-type' motif on either side that adopts same (in case of alpha-helix and beta-sheet) or adjacent (in case of loop) secondary structure component as residues of the motif. These residues along with the motif, hereafter referred as 'extended motifs' were used for exploring the binding site between the substrate proteins and hsc70 SBDα.

AlphaFold 3 was utilized to predict the structure of the complex between the peptides with extended motifs and the lid domain of hsc70. To check the stability of these complexes, each of them were subjected to 1 μs of all-atom MD simulations, generating a total of 15 μs of data. Interestingly, compared to the previous case wherein only 'KFERQ-type' motifs were explored,

the extended motifs demonstrated structural stability of the complex. The minimum distance between the substrate and the receptor protein remained below 2.5Å, indicating stable binding during the timescale of MD simulations (Figure 1E and Fig. S1B). The residues of hsc70 involved in the interaction with the residues of the substrate during the last 200 ns of the simulations are illustrated in Figure 1E. It was observed that the simulations stabilize all the proteins to site 1 of hsc70. To investigate whether the observed binding stability was an artifact of a particular force field or a general phenomenon, we performed simulations of the two of the complexes generated by AlphaFold 3 (PARK7 and α-Synuclein) using multiple force fields (CHARMM36, AMBER, and OPLS) with varying parameterization schemes. It was observed that the substrates are bound throughout the trajectory (Figure 1F). Overall, across all tested force fields, the binding remained intact, suggesting that the interaction is robust and not specific to any single force field. This consistency enhances confidence in the accuracy of the binding site prediction and its relevance under physiological conditions. Furthermore, the site is in agreement with the previous proposed model based on cross-linking experiments between human hsc70, yeast ssa1p and α-Synuclein[33].

To evaluate the contribution of adjacent residues to the stability of the 'KFERQ-type' motifs in the bound state, we removed the adjacent residues after they had participated in forming a complex with the motif and the chaperone i.e. adjacent residues flanking the motif were removed from the bound complexes in four of the previous runs (RND3, CHK1, PKM and PARK7) and the resulting complexes were subjected to MD simulations. The time evolution of the distance between substrate and receptor was monitored thereafter to check the stability of the complexes, Figure 1G. None of the complexes remained stable at the same site. The substrate disengaged from the proposed binding region and relocated to alternate positions. These findings indicate that the binding

interactions may not have been sufficiently robust. Taken together, our data suggests that additional residues adjacent to 'KFERQ-type' motif appear to play a crucial role in stabilizing the complex with the lid domain of Hsc70 under the conditions studied.

While it is well-established that the pentapeptide peptide motif in substrates is both necessary and sufficient for performing its CMA activity[36], our MD simulations suggest that the stability of the interaction between substrate and the lid domain of hsc70 may be influenced by the presence of additional adjacent residues. These residues could play a role in stabilizing the conformation required for effective interaction in a chaperone complex. This implies that while the motif is sufficient for activity, its stability and functionality might be enhanced under specific cellular conditions by adjacent residues. The finding also opened the door to exploring additional stabilizing factors present in the cellular environment.

CMA-targeting motifs in substrate proteins have selective affinity to hydrophobic cavity formed by helix α1 and helix α3 in SBDα of hsc70

To delve deeper into the binding site and interaction pattern, the binding pocket in hsc70 and the nature of interacting residues were identified. Figure 2A depicts a chord plot representing the residues involved in interaction. It was observed that interacting residues belong to helix *α1* and helix *α3* of SBD*α* in hsc70. Following an extensive analysis of the trajectories, we identified a set of receptor residues that consistently participated in interactions across majority of the simulated complexes, Figure 2A. These residues include Tyr545, Asn548, Met549, Asp555, Lys557, Leu558, Lys561, Glu600, Asn604, Ile607, Leu610, Tyr611, which were involved in stabilizing the binding through van der Waals interactions. Notably, Ile607 and Tyr611 emerged as critical hotspots, forming persistent interactions with the peptide in over 8 of the complexes. The conservation of these interaction patterns across the majority of systems underscores their potential significance in

maintaining the binding and highlights their role in the structural integrity of the receptor-substrate complex. This consistency suggests that these residues could be key determinants of binding specificity and stability, making them promising candidates for future mutational or experimental validation studies.

The contribution of each hsc70 residue towards stabilizing the binding interactions were analyzed by performing free energy calculations using MM-PBSA (Molecular Mechanics-Poisson Boltzmann Surface Area) approach. Figure 2B showcases the binding energies of residues with values more negative than -2.5 kcal/mol. Most of the residues are consistent with our occupancy analysis above. The common residues of occupancy and binding energy analysis include Tyr545, Asn548, Thr552, Leu558, Lys561, Glu600, Ile607, Leu610, and Tyr611. We propose the significance of these residues in rendering stabilization to the complex. Further, the identified residues in hsc70 encompassing the site contribute to the formation of a cavity with hydrophobic interior and hydrophilic exterior. The site can accommodate the side chains of hydrophobic amino acids of the peptide segment.

CMA-targeting motifs in substrate proteins display promiscuous orientation in the binding hydrophobic cavity

The stabilizing interactions between the substrate and chaperone within the selective binding site were examined in greater detail. Interestingly, despite the substrate consistently associated with the designated binding pocket, a comprehensive analysis of interaction patterns revealed a lack of reproducible stabilizing contacts across simulations of different substrates. Quantitative analysis, including calculating the contact frequencies and interaction energy underscores this observation (Figure 2A and 3A respectively). The hydrophobic side chains of the substrate exhibited varying interactions with the chaperone's binding pocket residues across different simulations. The

minimum distance between key interacting pairs is depicted in Fig. S2. These interactions were stable with the value ranging within 4Å. However, no consistent pair was identified in all the simulations, with the substrate adopting different binding modes in each simulation, leading to variable contact patterns with the binding site, as also evident from Figure 3B. This variability indicates that, while the substrate binds selectively to the hydrophobic pocket, the mode of binding demonstrates considerable flexibility. The absence of a consistent interaction pattern suggests a promiscuous nature of substrate-chaperone binding, which may be essential for accommodating diverse substrates within a shared binding site. These results collectively highlight the dual characteristics of binding: high specificity for the binding site but a lack of rigid interaction specificity.

When simulations were performed using different force fields, this dual characteristic of binding was consistently observed. While the substrate exhibited high specificity for the binding site across all force fields, the nature and dynamics of individual interactions varied significantly (Figure 3C and Fig. S3). Certain force fields emphasized stronger hydrophobic contacts, while others resulted in a more diverse range of transient interactions. These differences highlight the role of force field parameters in capturing the flexibility of substrate binding modes, suggesting that the observed promiscuity may be an inherent property of the system rather than an artifact of a specific simulation setup. Overall, based on our findings, we propose that the hydrophobic interactions in the hydrophobic cleft account for the substrate specificity while substrate promiscuity could be the result of induced-fit effects.

The current work proposed the binding site based on a peptide segment with an extended CMA-substrate motif. While there exists a possibility that the site might differ if we consider the full-length substrate, the consistent convergence of results across all tested substrates, across multiple

force fields, and supporting evidence from existing literature, strongly suggest that the identified interactions are robust and biologically relevant, providing valuable insights into the underlying recognition mechanism. Further structural and functional studies on full-length substrates and full-length hsc70 are essential to fully elucidate the substrate binding mechanism of Hsc70. Our work highlighted the significance of hydrophobic residues in CMA-recognition motifs of substrates. We could not observe specific binding roles of hydrophilic, positively and negatively charged residues, probably due to simplified truncated system of hsc70 used. The study opens the door to future explorations of these residues with respect to full length hsc70. The native structure of the substrates typically has hydrophobic residues within KFERQ-type motif and its flanking regions buried within the core. This suggests that partially unfolded states, where these hydrophobic residues become exposed, represent the binding-competent states for interaction with Hsc70. Our study paves the way for further investigations in this direction. Additionally, our findings highlight the need to explore diverse binding sites within the Hsp70 family to uncover potential evolutionary adaptations that fine-tune substrate interactions.

The methodology established in this study can be expanded to explore protein-protein binding interactions in other systems, especially those involving partially unfolded binding partners. This framework offers a robust approach for identifying interaction sites, understanding the structural adaptations necessary for binding, and uncovering the underlying principles of such dynamic interactions, post AlphaFold era.

Conclusion

The common binding site of 15 experimentally verified human CMA substrates in SBDα of Hsc70 was identified using a combination of bioinformatics approach, AlphaFold 3 predictions and molecular dynamic simulations. The results revealed that hydrophobic interactions drive substrate

recognition and specificity, and hsc70-substrate stabilization. The hydrophobic residues residing in the CMA-targeting motif and regions flanking the motif together provide the necessary stabilization. The findings have significant implications in targeted therapeutics. The pipeline designed in the current study can be extended to other systems to map protein-protein binding interactions wherein partially unfolded binding partners are involved.

Methods

Selection of segments in receptor and substrate proteins for exploring the binding site

In this study, specific parts of HSC70 and CMA substrates were focused on avoiding complexity. For Hsc70 the SBDα domain along with the C-terminal extension (residue 510 to 646) is kept as this part is the possible site for binding substrates. Fifteen experimentally verified CMA substrates were taken considering the following criteria 1) come from human origin and 2) include a single KFERQ-like motif. To identify KFERQ motifs in substrate proteins, we used the KFERQ finder V0.8 tool [10]. The secondary structures of these proteins were determined using the STRIDE[37] program, applied to structures obtained from the Protein Data Bank (PDB) and AlphaFold database[38–40].

Protein complex prediction with AlphaFold 3

To determine the binding sites between hsc70 and CMA substrates, we have utilized AlphaFold 3[31]. The models with the highest iPTM score among the five models generated for each system were taken for further analysis.

Molecular Dynamics Simulations

To explore the stability of protein-protein interactions predicted using AlphaFold 3, all-atom MD simulations were performed using the GROMACS 2020.4 package for each model of hsc70-CMA substrate complexes [41]. CHARMM36 force field was used to simulate protein complexes [42,43]. Preparation of initial systems was done by assigning standard protonation states to the ionizable residues corresponding to pH 7 using PropKa[44]. Cubic box with a gap of 10 Å between the surface of the protein complex and the edge was defined. Systems were solvated using TIP3P water model and neutralized by NaCl[45]. Energy minimization was done using Steepest Descent algorithm until the energy difference between steps was less than 1000 kJ mol^{-1} nm^{-1}[46]. Two-step equilibration was performed, first using the NVT ensemble, followed by the NPT ensemble. The temperature was controlled to 300 K by a V-rescale thermostat [47] and pressure to 1 bar using the Parrinello–Rahman barostat[48]. A time step of 2 fs was used and at every 100 steps coordinates were written. Amber as well as OPLS force fields were used for two complexes (alpha-Synuclein and PARK7) to analyze the effect of force fields[49,50]. The analysis was carried out either using in-build gromacs utilities or in-house scripts.

Figure legends

Figure 1. Residues adjacent to the 'CMA-targeting' motif stabilizes its binding with hsc70. (**A**) Heatmap representing the residues of hsc70 lid domain interacting with 'KFERQ-type' motifs in AlphaFold 3 predicted complexes for 15 CMA substrates. Three different sites were observed (site-1 in light sea green, site-2 in pink, and site-3 in goldenrod). (**B**) 3D surface representation of the lid domain of hsc70 depicting the three predicted binding sites. The loop region in the lid domain is not shown for clarity. (**C**) Minimum distance between hsc70 lid domain and CMA substrate peptides with only 'KFERQ-type' motif. It represents structural instability of the complex during the course of MD simulations. (**D**) Schematic representation of secondary structure of CMA-

targeting motifs along with adjacent amino acid residue of 15 CMA substrates that were taken for binding site predictions (termed as 'extended CMA-targeting motifs'). (**E**) Heatmap representing the interacting residues of the hsc70 lid domain with extended CMA-targeting motifs (Top panel), accompanied by corresponding minimum distance plot between the two (Bottom panel), averaged over last 200 ns. Surface representation of hsc70 lid domain with the interacting side highlighted in purple (loop region is not shown for clarity). The binding site remained stable throughout the simulations. (**F**) Minimum distance plots of hsc70 lid domain and extended CMA-targeting motifs in PARK7 and α-Synuclein using AMBER, OPLS, and CHARMM 36 force fields. A value below 2.5 Å indicates stability in each force field. (**G**) Minimum distance between hsc70 and RND3, CHK1, PKM and PARK7 peptide in the complexes. The complexes were generated by removing the adjacent residues in CMA substrates after they had participated in forming a complex with the motif and the chaperone. None of the complexes remained stable.

Figure 2. CMA-targeting motifs selectively bind to the hydrophobic cavity formed by helix α1 and helix α3 in the lid domain of hsc70. (**A**) A chord diagram representing the residues of hsc70 lid domain interacting with amino acid segments from 15 CMA substrates, where the thickness of the node for each respective residue represents the frequency of interactions. Residues of helices α1 and α3 are extensively participating for interactions with substrate segment (also depicted in cartoon representations at the bottom). (**B**) Binding energies of hsc70 residues below -2.5 kcal/mol (left panel, calculated using MMPBSA) are shown alongside a lipophilic representation of the cavity (right panel). Key interacting residues are depicted in ball-and-stick representation.

Figure 3. CMA-targeting motifs in substrate proteins display promiscuous orientation in the binding hydrophobic cavity. (**A**) Residue-wise decomposition of binding energies of CMA substrates peptides. Only residues with values less than -2.5 kcal/mol are shown. (**B**) Orientation

of CMA substrate peptides within the hydrophobic cavity of hsc70, with the substrate segment depicted in gray cartoon representation. (**C**) Residue-wise decomposition of binding energies of PARK7 and α-Synuclein using three different force fields (Amber, OPLS, and CHARMM36), with different values in each force field indicating the flexibility of substrate binding modes. Residues which are part of CMA-targeting motif are represented by red color.

Figure 1

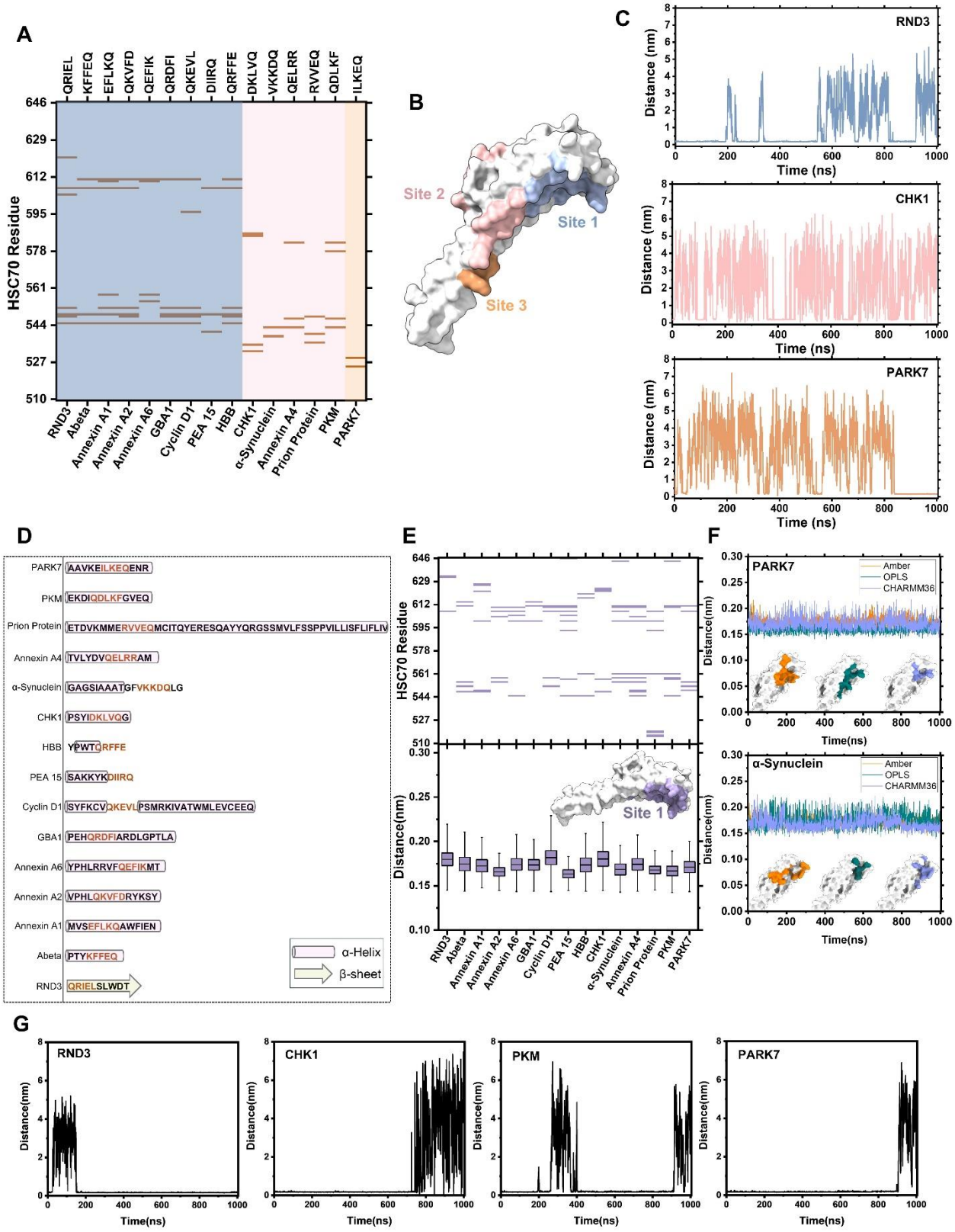
A
QRIEL
KFFEQ
EFLKQ
QKVFD
QEFIK
QRDFI
QKEVL
DIIRQ
QRFFE
DKLVQ
VKKDQ
QELRR
RVVEQ
QDLKF
ILKEQ
HSC70 Residue
RND3
Abeta
Annexin A1
Annexin A2
Annexin A6
GBA1
Cyclin D1
PEA 15
HBB
CHK1
α-Synuclein
Annexin A4
Prion Protein
PKM
PARK7
B
Site 2
Site 1
Site 3
C
RND3
CHK1
PARK7
Distance (nm)
Time (ns)
D
PARK7 AAVKEILKEQENR
PKM EKDIQDLKFGVEQ
Prion Protein ETDVKMMERVVEQMCITQYERESQAYYQRGSSMVLFSSPPVILLISFLIFLIV
Annexin A4 TVLYDVQELRRAM
α-Synuclein GAGSIAAATGFVKKDQLG
CHK1 PSYIDKLVQG
HBB YPWTQRFFE
PEA 15 SAKKYKDIIRQ
Cyclin D1 SYFKCVQKEVLPSMRKIVATWMLEVCEEQ
GBA1 PEHQRDFIARDLGPTLA
Annexin A6 YPHLRRVFQEFIKMT
Annexin A2 VPHLQKVFDRYKSY
Annexin A1 MVSEFLKQAWFIEN
Abeta PTYKFFEQ
RND3 QRIELSLWDT
α-Helix
β-sheet
E
HSC70 Residue
Distance(nm)
Site 1
F
PARK7
α-Synuclein
Amber
OPLS
CHARMM36
Distance(nm)
Time(ns)
G
RND3
CHK1
PKM
PARK7
Distance(nm)
Time(ns)

Figure 2

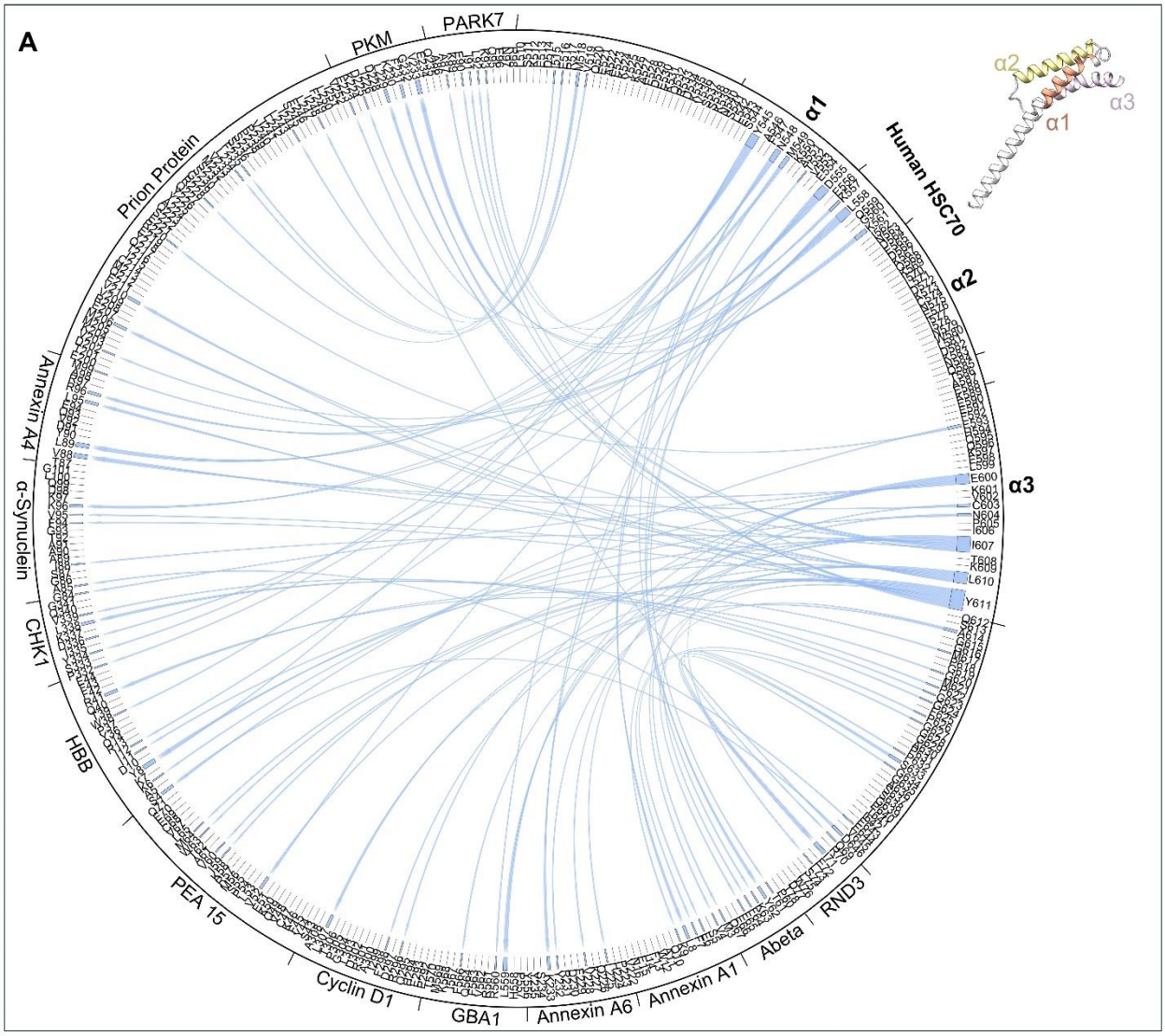
A
PARK7
PKM
Prion Protein
Annexin A4
α-Synuclein
CHK1
HBB
PEA 15
Cyclin D1
GBA1
Annexin A6
Annexin A1
Abeta
RND3
Human HSC70
α1
α2
α3
α2
α3
α1

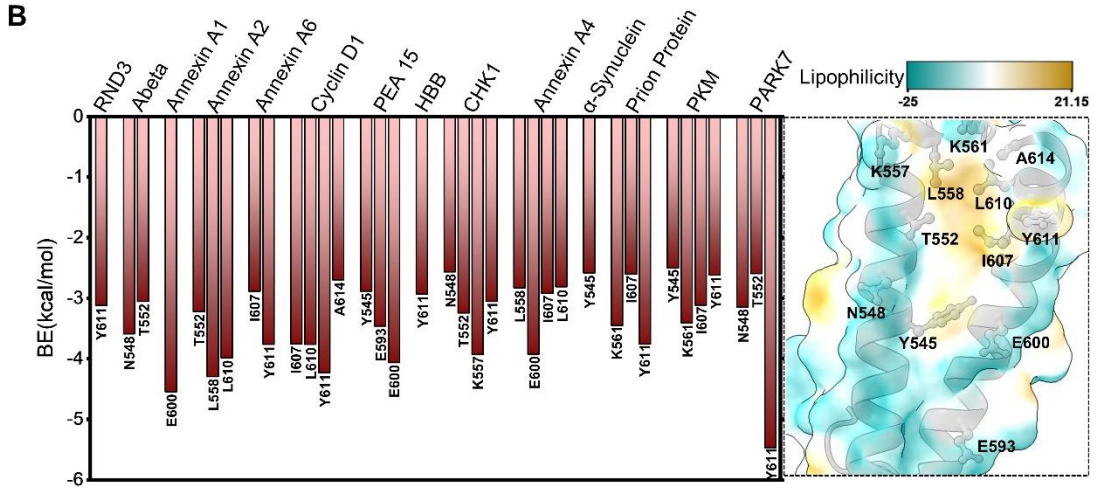
B
RND3
Abeta
Annexin A1
Annexin A2
Annexin A6
Cyclin D1
PEA 15
HBB
CHK1
Annexin A4
α-Synuclein
Prion Protein
PKM
PARK7
Lipophilicity
-25
21.15
BE(kcal/mol)
0
-1
-2
-3
-4
-5
-6
K561
A614
K557
L558
L610
T552
Y611
I607
N548
Y545
E600
E593

Figure 3

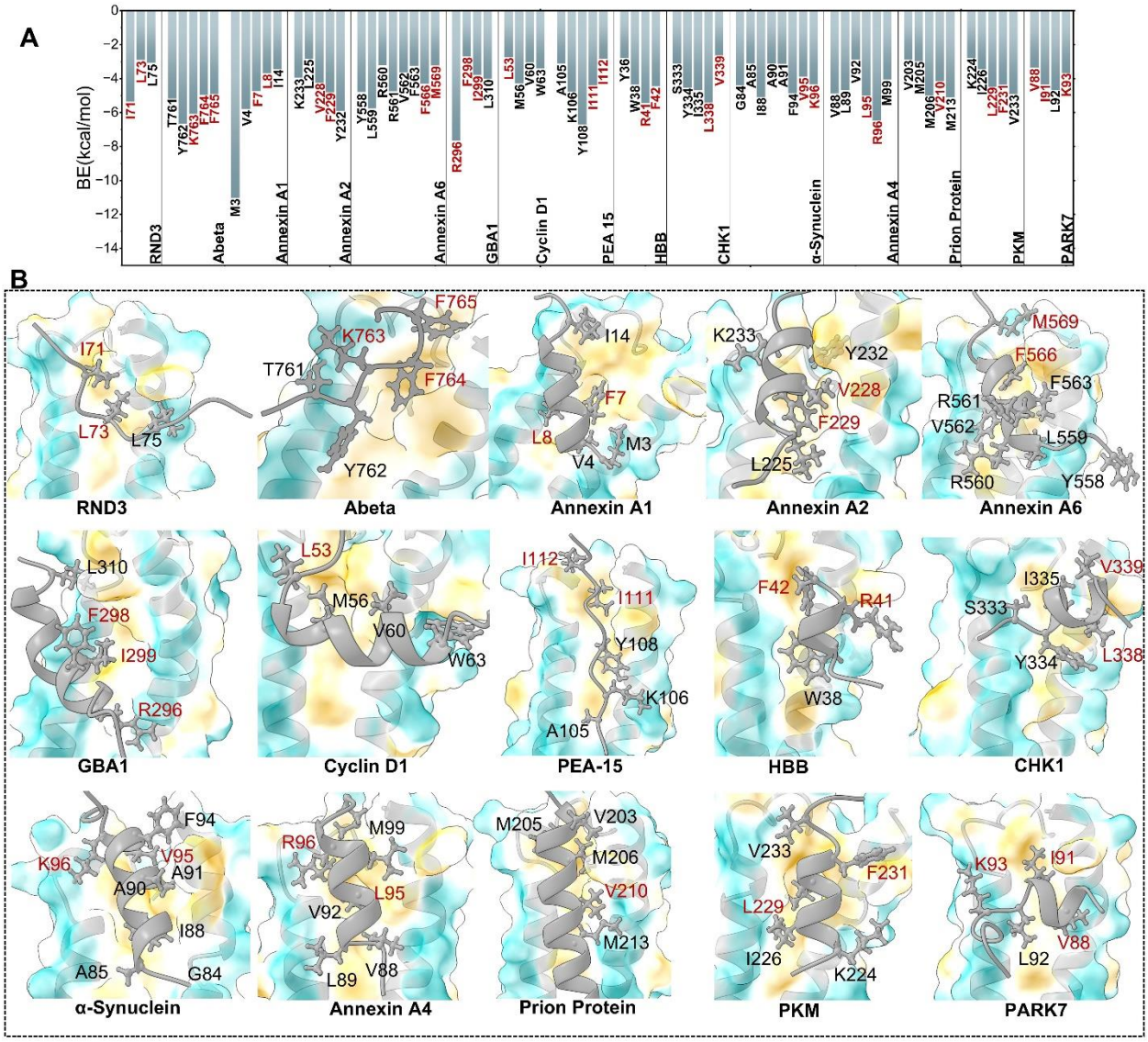
A
BE(kcal/mol)
RND3
Abeta
Annexin A1
Annexin A2
Annexin A6
GBA1
Cyclin D1
PEA 15
HBB
CHK1
α-Synuclein
Annexin A4
Prion Protein
PKM
PARK7
B
RND3
Abeta
Annexin A1
Annexin A2
Annexin A6
GBA1
Cyclin D1
PEA-15
HBB
CHK1
α-Synuclein
Annexin A4
Prion Protein
PKM
PARK7

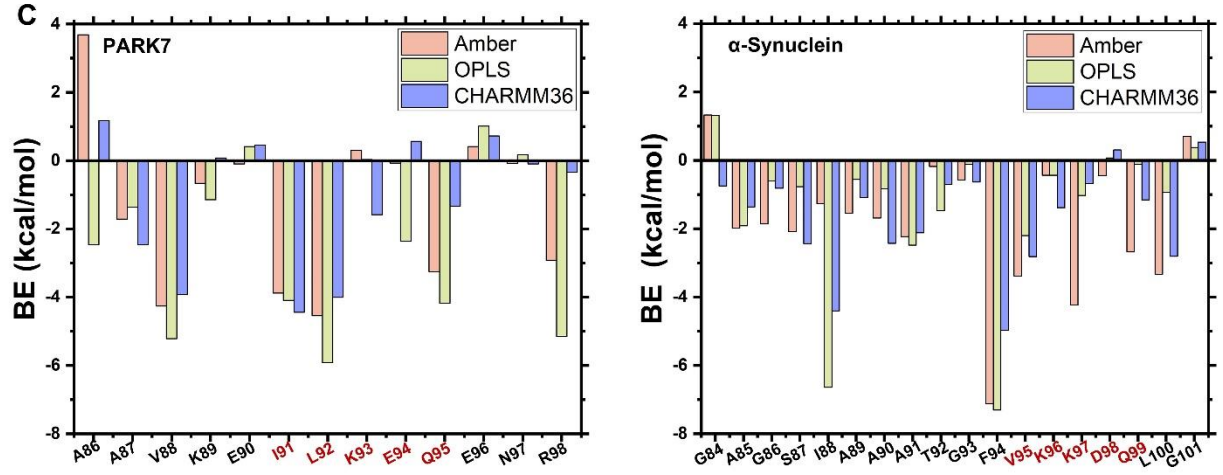
C
PARK7
Amber
OPLS
CHARMM36
BE (kcal/mol)
A86 A87 V88 K89 E90 I91 L92 K93 E94 Q95 E96 N97 R98
α-Synuclein
Amber
OPLS
CHARMM36
BE (kcal/mol)
G84 A85 G86 S87 I88 A89 A90 A91 T92 G93 F94 V95 K96 K97 D98 G99 L100 G101

Acknowledgements

N.M. acknowledges the financial support from the Shiv Nadar Foundation and the DST Inspire Faculty Grant [DST/INSPIRE/04/2022/001599]. D.S. acknowledges the junior research fellowship from the Shiv Nadar Foundation.

Disclosure statement

The authors declare that they have no known competing financial interests or personal relationships that could have appeared to influence the work reported in this paper.

Funding

The work was supported by Shiv Nadar Foundation and the DST Inspire Faculty Grant [DST/INSPIRE/04/2022/001599]

Data availability statement

The data files related to this study have been made available at: https://github.com/CSBLabNM/Project_HSC70.git

References

[1] Massey A, Kiffin R, Cuervo AM. Pathophysiology of chaperone-mediated autophagy. Int J Biochem Cell Biol. 2004;36(12):2420–2434.

[2] Vélez EJ, Schnebert S, Goguet M, et al. Chaperone-mediated autophagy protects against hyperglycemic stress. Autophagy. 2024;20(4):752–768.

[3] Massey AC, Zhang C, Cuervo AM. Chaperone-Mediated Autophagy in Aging and Disease. 2006. p. 205–235.

[4] Koga H, Cuervo AM. Chaperone-mediated autophagy dysfunction in the pathogenesis of neurodegeneration. Neurobiol Dis. 2011;43(1):29–37.

[5] Wu J, Xu W, Su Y, et al. Targeting chaperone-mediated autophagy in neurodegenerative diseases: mechanisms and therapeutic potential. Acta Pharmacol Sin. 2024; doi: 10.1038/s41401-024-01416-3.

[6] Dice JF. Peptide sequences that target cytosolic proteins for lysosomal proteolysis. Trends Biochem Sci. 1990;15(8):305–309.

[7] Chiang H-L, Terlecky SR, Plant CP, et al. A Role for a 70-Kilodalton Heat Shock Protein in Lysosomal Degradation of Intracellular Proteins. Science (1979). 1989;246(4928):382–385.

[8] Cuervo AM, Terlecky SR, Dice JF, et al. Selective binding and uptake of ribonuclease A and glyceraldehyde-3-phosphate dehydrogenase by isolated rat liver lysosomes. J Biol Chem. 1994;269(42):26374–26380.

[9] Koga H, Martinez-Vicente M, Macian F, et al. A photoconvertible fluorescent reporter to track chaperone-mediated autophagy. Nat Commun. 2011;2(1):386.

[10] Kirchner P, Bourdenx M, Madrigal-Matute J, et al. Proteome-wide analysis of chaperone-mediated autophagy targeting motifs. PLoS Biol. 2019;17(5):e3000301.

[11] Lv L, Li D, Zhao D, et al. Acetylation targets the M2 isoform of pyruvate kinase for degradation through chaperone-mediated autophagy and promotes tumor growth. Mol Cell. 2011;42(6):719–730.

[12] Bonhoure A, Vallentin A, Martin M, et al. Acetylation of translationally controlled tumor protein promotes its degradation through chaperone-mediated autophagy. Eur J Cell Biol. 2017;96(2):83–98.

[13] Kaushik S, Cuervo AM. Degradation of lipid droplet-associated proteins by chaperone-mediated autophagy facilitates lipolysis. Nat Cell Biol. 2015;17(6):759–770.

[14] Kirchner P, Bourdenx M, Madrigal-Matute J, et al. Correction: Proteome-wide analysis of chaperone-mediated autophagy targeting motifs. PLoS Biol. 2022;20(2):e3001550.

[15] Kaushik S, Cuervo AM. The coming of age of chaperone-mediated autophagy. Nat Rev Mol Cell Biol. 2018;19(6):365–381.

[16] Majeski AE, Fred Dice J. Mechanisms of chaperone-mediated autophagy. Int J Biochem Cell Biol. 2004;36(12):2435–2444.

[17] Wang D, Peng Z, Ren G, et al. The different roles of selective autophagic protein degradation in mammalian cells. Oncotarget. 2015;6(35):37098–37116.

[18] Robert G, Jacquel A, Auberger P. Chaperone-Mediated Autophagy and Its Emerging Role in Hematological Malignancies. Cells. 2019;8(10):1260.

[19] Cuervo AM, Gomes A V., Barnes JA, et al. Selective Degradation of Annexins by Chaperone-mediated Autophagy. Journal of Biological Chemistry. 2000;275(43):33329–33335.

[20] Gomes LR, Menck CFM, Cuervo AM. Chaperone-mediated autophagy prevents cellular transformation by regulating MYC proteasomal degradation. Autophagy. 2017;13(5):928–940.

[21] Tang Y, Wang X-W, Liu Z-H, et al. Chaperone-mediated autophagy substrate proteins in cancer. Oncotarget. 2017;8(31):51970–51985.

[22] Qi R, Sarbeng EB, Liu Q, et al. Allosteric opening of the polypeptide-binding site when an Hsp70 binds ATP. Nat Struct Mol Biol. 2013;20(7):900–907.

[23] Bertelsen EB, Chang L, Gestwicki JE, et al. Solution conformation of wild-type *E. coli* Hsp70 (DnaK) chaperone complexed with ADP and substrate. Proceedings of the National Academy of Sciences. 2009;106(21):8471–8476.

[24] Cupp-Vickery JR, Peterson JC, Ta DT, et al. Crystal Structure of the Molecular Chaperone HscA Substrate Binding Domain Complexed with the IscU Recognition Peptide ELPPVKIHC. J Mol Biol. 2004;342(4):1265–1278.

[25] Zahn M, Berthold N, Kieslich B, et al. Structural Studies on the Forward and Reverse Binding Modes of Peptides to the Chaperone DnaK. J Mol Biol. 2013;425(14):2463–2479.

[26] Tapley TL, Cupp-Vickery JR, Vickery LE. Sequence-Dependent Peptide Binding Orientation by the Molecular Chaperone DnaK. Biochemistry. 2005;44(37):12307–12315.

[27] Zhu X, Zhao X, Burkholder WF, et al. Structural Analysis of Substrate Binding by the Molecular Chaperone DnaK. Science (1979). 1996;272(5268):1606–1614.

[28] Johnson OT, Gestwicki JE. Multivalent protein-protein interactions are pivotal regulators of eukaryotic Hsp70 complexes. Cell Stress Chaperones. 2022;27(4):397–415.

[29] Taylor IR, Ahmad A, Wu T, et al. The disorderly conduct of Hsc70 and its interaction with the Alzheimer's-related Tau protein. Journal of Biological Chemistry. 2018;293(27):10796–10809.

[30] Nachman E, Wentink AS, Madiona K, et al. Disassembly of Tau fibrils by the human Hsp70 disaggregation machinery generates small seeding-competent species. Journal of Biological Chemistry. 2020;295(28):9676–9690.

[31] Abramson J, Adler J, Dunger J, et al. Accurate structure prediction of biomolecular interactions with AlphaFold 3. Nature. 2024;630(8016):493–500.

[32] Nury C, Redeker V, Dautrey S, et al. A Novel Bio-Orthogonal Cross-Linker for Improved Protein/Protein Interaction Analysis. Anal Chem. 2015;87(3):1853–1860.

[33] Redeker V, Pemberton S, Bienvenut W, et al. Identification of Protein Interfaces between α-Synuclein, the Principal Component of Lewy Bodies in Parkinson Disease, and the Molecular Chaperones Human Hsc70 and the Yeast Ssa1p. Journal of Biological Chemistry. 2012;287(39):32630–32639.

[34] Fox-Erlich S. Structural conservation of a short, functional, peptide-sequence motif. Frontiers in Bioscience. 2009;Volume(14):1143.

[35] Popelka H, Klionsky DJ. Structural basis for extremely strong binding affinity of giant ankyrins to LC3/GABARAP and its application in the inhibition of autophagy. Autophagy. 2018;14(11):1847–1849.

[36] Dice JF, Chiang HL, Spencer EP, et al. Regulation of catabolism of microinjected ribonuclease A. Identification of residues 7-11 as the essential pentapeptide. J Biol Chem. 1986;261(15):6853–6859.

[37] Heinig M, Frishman D. STRIDE: a web server for secondary structure assignment from known atomic coordinates of proteins. Nucleic Acids Res. 2004;32(Web Server):W500–W502.

[38] Burley SK, Bhatt R, Bhikadiya C, et al. Updated resources for exploring experimentally-determined PDB structures and Computed Structure Models at the RCSB Protein Data Bank. Nucleic Acids Res. 2025;53(D1):D564–D574.

[39] Berman HM. The Protein Data Bank. Nucleic Acids Res. 2000;28(1):235–242.

[40] Jumper J, Evans R, Pritzel A, et al. Highly accurate protein structure prediction with AlphaFold. Nature. 2021;596(7873):583–589.

[41] Abraham MJ, Murtola T, Schulz R, et al. GROMACS: High performance molecular simulations through multi-level parallelism from laptops to supercomputers. SoftwareX. 2015;1–2:19–25.

[42] Huang J, MacKerell AD. CHARMM36 all-atom additive protein force field: Validation based on comparison to NMR data. J Comput Chem. 2013;34(25):2135–2145.

[43] Vanommeslaeghe K, Hatcher E, Acharya C, et al. CHARMM general force field: A force field for drug-like molecules compatible with the CHARMM all-atom additive biological force fields. J Comput Chem. 2010;31(4):671–690.

[44] Jurrus E, Engel D, Star K, et al. Improvements to the <scp>APBS</scp> biomolecular solvation software suite. Protein Science. 2018;27(1):112–128.

[45] Jorgensen WL, Chandrasekhar J, Madura JD, et al. Comparison of simple potential functions for simulating liquid water. J Chem Phys. 1983;79(2):926–935.

[46] Debye P. N□herungsformeln f□r die Zylinderfunktionen f□r gro□e Werte des Arguments und unbeschr□nkt ver□nderliche Werte des Index. Math Ann. 1909;67(4):535–558.

[47] Bussi G, Donadio D, Parrinello M. Canonical sampling through velocity rescaling. J Chem Phys. 2007;126(1).

[48] Parrinello M, Rahman A. Polymorphic transitions in single crystals: A new molecular dynamics method. J Appl Phys. 1981;52(12):7182–7190.

[49] Maier JA, Martinez C, Kasavajhala K, et al. ff14SB: Improving the Accuracy of Protein Side Chain and Backbone Parameters from ff99SB. J Chem Theory Comput. 2015;11(8):3696–3713.

[50] Kaminski GA, Friesner RA, Tirado-Rives J, et al. Evaluation and Reparametrization of the OPLS-AA Force Field for Proteins via Comparison with Accurate Quantum Chemical Calculations on Peptides. J Phys Chem B. 2001;105(28):6474–6487.

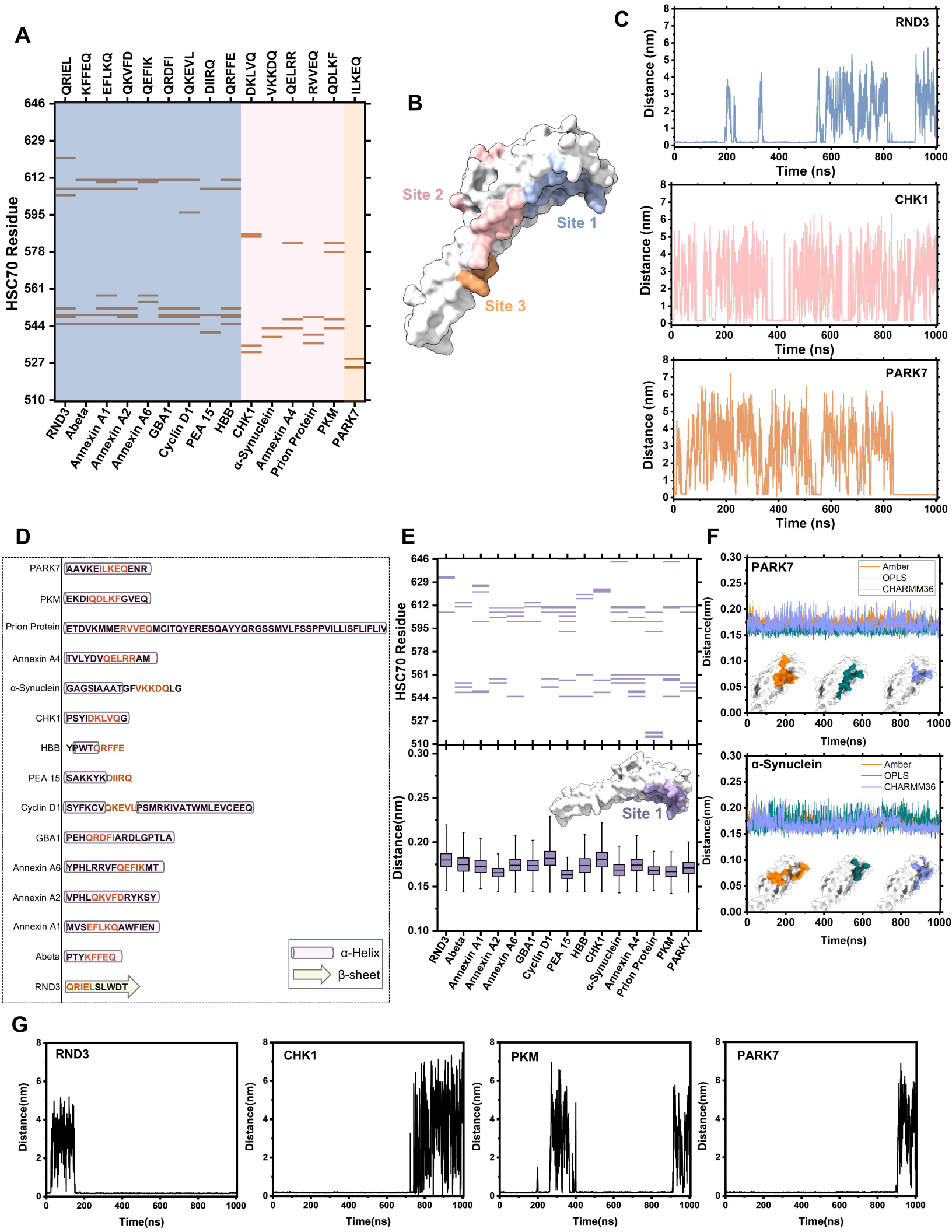
A
QRIEL
KFFEQ
EFLKQ
QKVFD
QEFIK
QRDFI
QKEVL
DIIRQ
QRFFE
DKLVQ
VKKDQ
QELRR
RVVEQ
QDLKF
ILKEQ
HSC70 Residue
RND3
Abeta
Annexin A1
Annexin A2
Annexin A6
GBA1
Cyclin D1
PEA 15
HBB
CHK1
α-Synuclein
Annexin A4
Prion Protein
PKM
PARK7
B
Site 1
Site 2
Site 3
C
RND3
CHK1
PARK7
Distance (nm)
Time (ns)
D
PARK7 AAVKEILKEQENR
PKM EKDIQDLKFGVEQ
Prion Protein ETDVKMMERVVEQMCITQYERESQAYYQRGSSMVLFSSPPVILLISFLIFLIV
Annexin A4 TVLYDVQELRRAM
α-Synuclein GAGSIAAATGFVKKDQLG
CHK1 PSYIDKLVQG
HBB YPWTQRFFE
PEA 15 SAKKYKDIIRQ
Cyclin D1 SYFKCVQKEVLPSMRKIVATWMLEVCEEQ
GBA1 PEHQRDFIARDLGPTLA
Annexin A6 YPHLRRVFQEFIKMT
Annexin A2 VPHLQKVFDRYKSY
Annexin A1 MVSEFLKQAWFIEN
Abeta PTYKFFEQ
RND3 QRIELSLWDT
α-Helix
β-sheet
E
HSC70 Residue
Distance(nm)
Site 1
F
PARK7
α-Synuclein
Amber
OPLS
CHARMM36
Distance(nm)
Time(ns)
G
RND3
CHK1
PKM
PARK7
Distance(nm)
Time(ns)

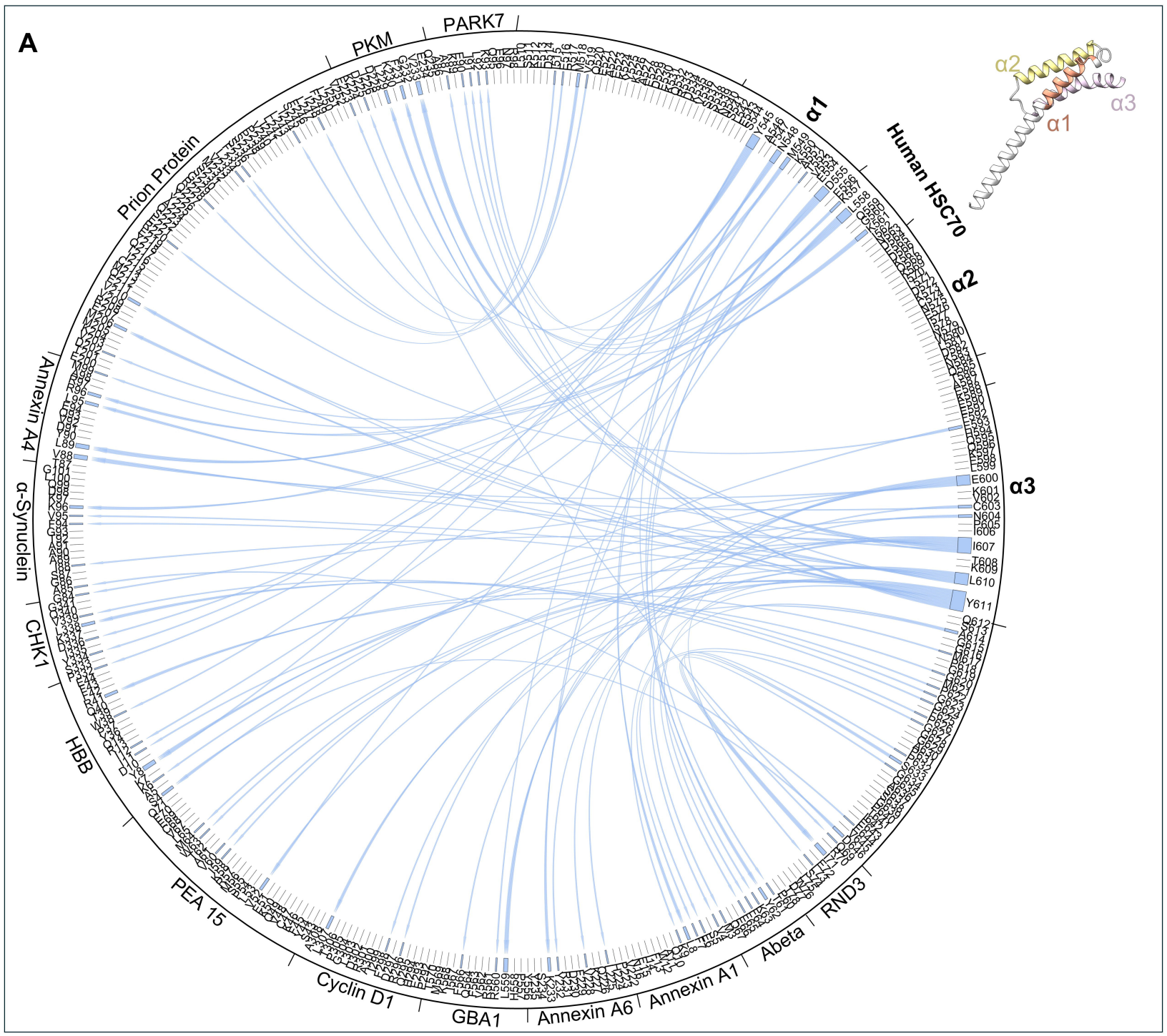
A
PARK7
PKM
Prion Protein
Annexin A4
α-Synuclein
CHK1
HBB
PEA 15
Cyclin D1
GBA1
Annexin A6
Annexin A1
Abeta
RND3
Human HSC70
α1
α2
α3
α2
α3
α1

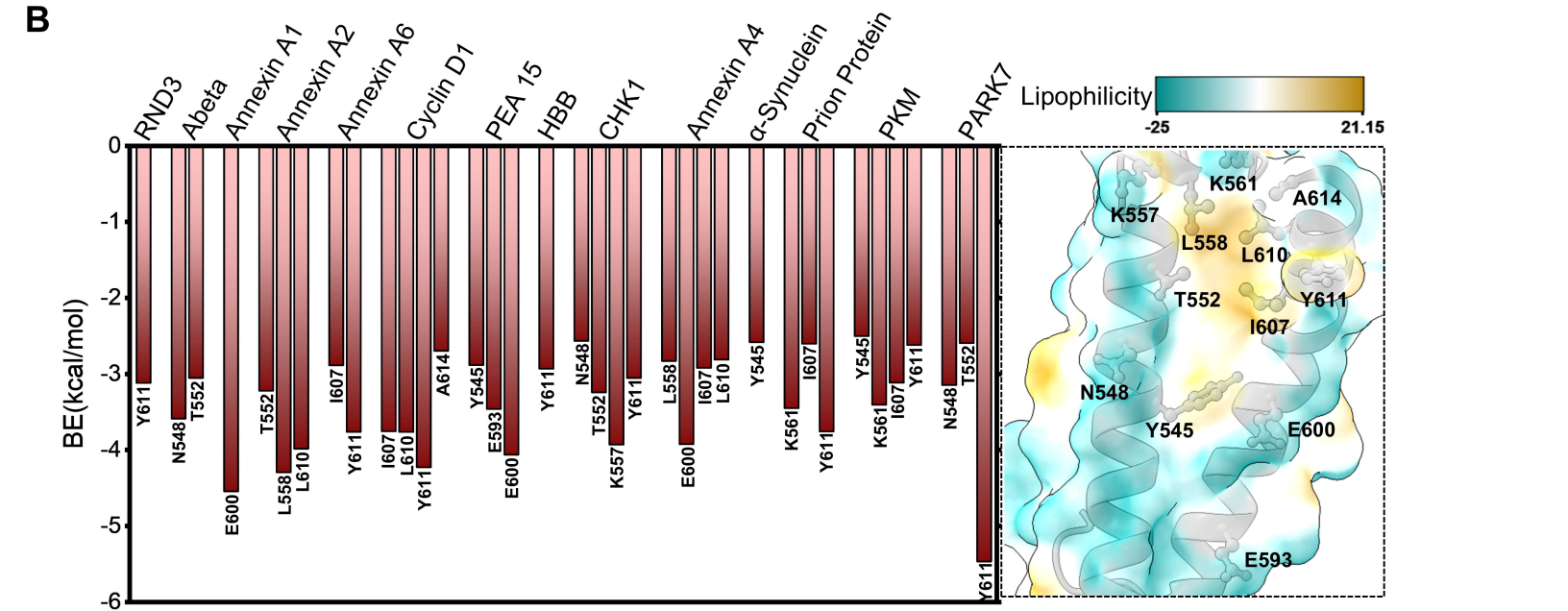
B
RND3
Abeta
Annexin A1
Annexin A2
Annexin A6
Cyclin D1
PEA 15
HBB
CHK1
Annexin A4
α-Synuclein
Prion Protein
PKM
PARK7
BE(kcal/mol)
0
-1
-2
-3
-4
-5
-6
Lipophilicity
-25
21.15
K561
A614
K557
L558
L610
T552
Y611
I607
N548
Y545
E600
E593

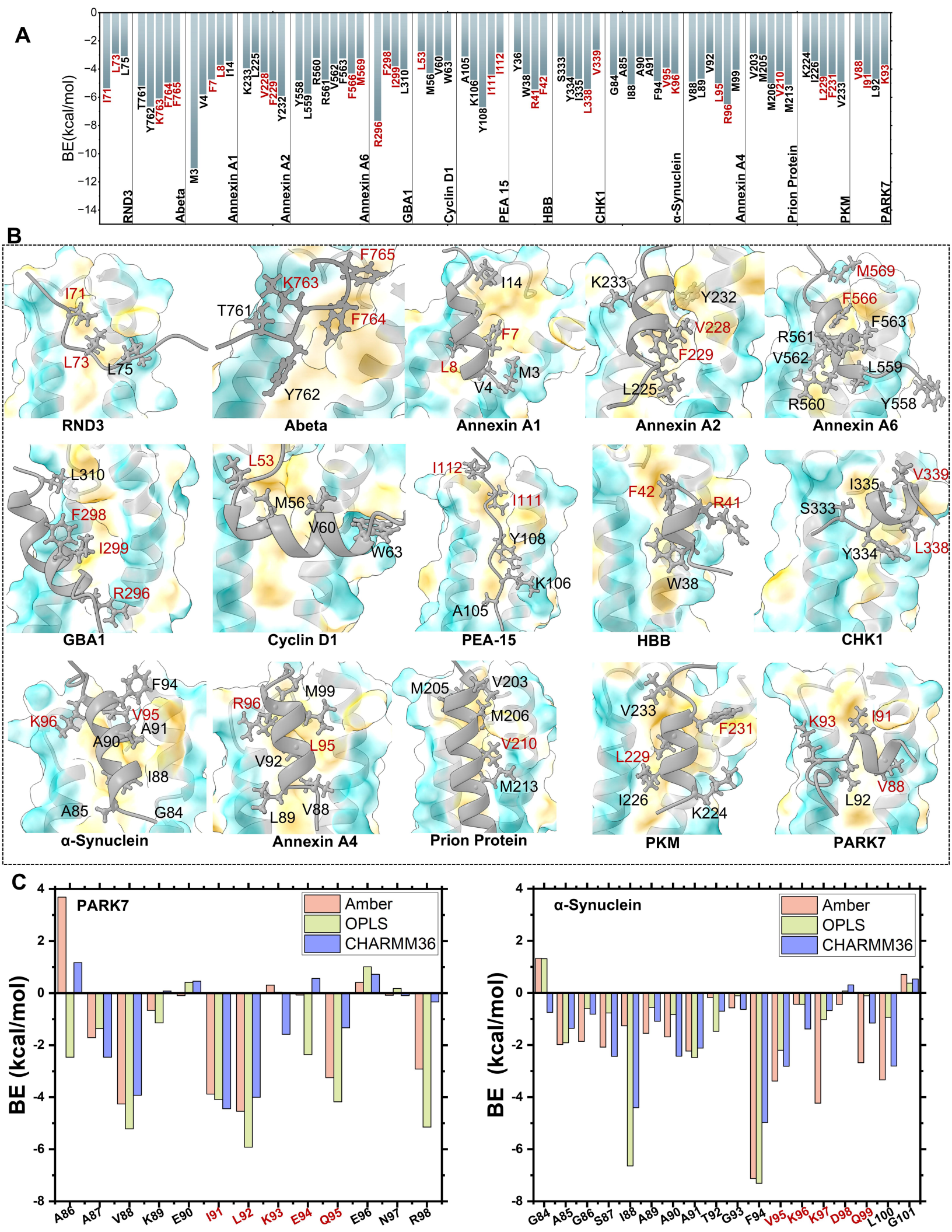
A
BE(kcal/mol)
0
−2
−4
−6
−8
−10
−12
−14
I71 L73 L75
RND3
T761 Y762 K763 F764 F765
Abeta
M3 V4 F7 L8 I14
Annexin A1
K233 L225 V228 F229 Y232
Annexin A2
Y558 L559 R560 R561 V562 F563 F566 M569
Annexin A6
R296 F298 I299 L310
GBA1
L53 M56 V60 W63
Cyclin D1
A105 K106 Y108 I111 I112
PEA 15
Y36 W38 R41 F42
HBB
S333 Y334 I335 L338 V339
CHK1
G84 A85 I88 A90 A91 F94 V95 K96
α-Synuclein
V88 L89 V92 L95 R96 M99
Annexin A4
V203 M205 M206 V210 M213
Prion Protein
K224 I226 I229 F231 V233
PKM
V88 I91 L92 K93
PARK7
B
I71
L73
L75
RND3
T761
K763
F765
F764
Y762
Abeta
I14
F7
L8
M3
V4
Annexin A1
K233
Y232
V228
F229
L225
Annexin A2
M569
F566
F563
R561
V562
L559
R560
Y558
Annexin A6
L310
F298
I299
R296
GBA1
L53
M56
V60
W63
Cyclin D1
I112
I111
Y108
K106
A105
PEA-15
F42
R41
W38
HBB
V339
I335
S333
Y334
L338
CHK1
F94
K96
V95
A91
A90
I88
A85
G84
α-Synuclein
M99
R96
L95
V92
V88
L89
Annexin A4
M205
V203
M206
V210
M213
Prion Protein
V233
F231
L229
I226
K224
PKM
K93
I91
V88
L92
PARK7
C
PARK7
Amber
OPLS
CHARMM36
BE (kcal/mol)
4
2
0
-2
-4
-6
-8
A86 A87 V88 K89 E90 I91 L92 K93 E94 Q95 E96 N97 R98
α-Synuclein
Amber
OPLS
CHARMM36
BE (kcal/mol)
4
2
0
-2
-4
-6
-8
G84 A85 G86 S87 I88 A89 A90 A91 T92 G93 F94 V95 K96 K97 D98 Q99 L100 G101